Stability and amyloid aggregation studies of exendin-4 analog miniproteins

PhD thesis

Dániel Horváth

Doctoral School of Pharmaceutical Sciences
Semmelweis University

Supervisor:
Dr. András Perczel D.Sc

Official reviewers:
Dr. László Smeller, D.Sc
Dr. Orsolya Tőke, Ph.D.

Head of the Final Examination Committee:
Dr. Romána Zelkó, D.Sc

Members of the Final Examination Committee:
Dr. Gergő Tóth, Ph.D.
Dr. Ádám Fizil, Ph.D.

Budapest, 2020

1. Introduction

Peptide and protein-based drugs play an ever increasing role in modern therapeutic practice. Due to their size and structural complexity, their production, analysis and formulation are complex and differ from those of small molecule drugs. Due to their chemical nature, their stability as well as bioavailability are limited in terms of both absorption and metabolism. However, using certain innovative technologies, such as rationally designed point mutations, incorporation of non-natural amino acids, fatty acid chain conjugations, post-translational modifications, the use of excipients, can increase the solubility and stability of the drug, as well as extend its shelf-life and circulating half-life. In the last 20 years, the number of people diagnosed with diabetes has tripled, mostly due to the increasing number of patients with type 2 diabetes. Another major challenge has become the treatment and prevention of neurodegenerative diseases common in aging societies. Development and progression of these widespread illnesses as well as one of the most common source of instabilities of protein and peptide-medications concerns the amyloid aggregation of proteins. Revealing and understanding the structure and formation of protein aggregate amyloid plaques is thus a key element in developing future therapeutic strategies.

The incretin mimetic GLP-1 analogs have been used successfully in the treatment of type 2 diabetes. In addition to their therapeutic effect, these miniproteins, despite their small size, have a tertiary structure, so in addition to the basic protein folding/unfolding processes and the effect of point mutations on the spatial structure can be studied at the atomic level. In addition, some derivatives show a tendency toward amyloid aggregation, so

that conformational changes during aggregation processes can also be monitored and characterized.

In my doctoral research, I studied a 25 amino acid long variant of Exenatide, a drug currently in use for the treatment of type-2 diabetes **(figure 1.)**

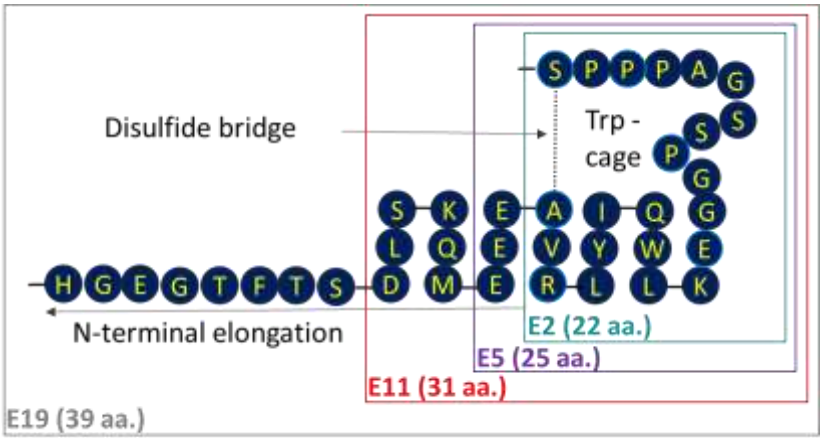

Figure 1. Sequence of Exenatide derived miniproteins with different lengths. For amino acids with a light blue border, there was a substitution in the sequence.

2. Aims

A) I planned to investigate the effect subtle changes (introduction of fluoroprolines, secondary ionic interactions, and the incorporation of a disulfide bridge) on the tertiary structure and thermal stability of E5. **(figure 2.)** My aim was also to compare the temperature dependent ECD and NMR spectroscopic data sets concerning these systems.

B) I aimed to characterize the structure and reduction kinetics of disulfide cyclized Exenatide derivatives of varying length (E2, E5, E11, E19- **figure 1.**) under different reduction conditions using spectroscopic methods.

C) My goal was to determine the biological activity of E19_SS in mammalian INS-1 cells.

D) I planned spectroscopic characterization of the amyloid aggregation of the E5 miniprotein. My goal was to determine the conformation of the monomer most prone to aggregate, the early stages of the process and the morphology of oligomers and amyloid fibers formed during elongation.

3. Methods

Peptides and miniproteins were prepared by bacterial expression or solid phase peptide synthesis and then purified by C18 reverse phase HPLC chromatography. **(figure 2.)**

Exenatide	HGEG TFTSD LSKQM EEEAV RLFIE WLKNG GPSSG APPPS
E5	EEEAV RLYIQ WLKEG GPSSG RPPPS
E5_E14D	EEEAV RLYIQ WLK**D**G GPSSG RPPPS
E5_E14Q	EEEAV RLYIQ WLK**Q**G GPSSG RPPPS
E5_A4C_E14D_S25C	EEE**C**V RLYIQ WLK**D**G GPSSG RPPP**C**
E5_R6N	EEEAV **N**LYIQ WLKEG GPSSG RPPPS
E5_E14D_P17(4S)fP	EEEAV RLYIQ WLK**D**G G**P**SSG RPPPS
E5_E14D_P17(4R)fP	EEEAV RLYIQ WLK**D**G G**P**SSG RPPPS
E5_E14D_P24(4S)fP	EEEAV RLYIQ WLK**D**G GPSSG RPP**P**S
E5_E14D_P24(4R)fP	EEEAV RLYIQ WLK**D**G GPSSG RPP**P**S
E2_SS/E2_2SH	CV RLYIQ WLKDG GPSSG RPPPC
E5_SS/E5_2SH	EEECV RLYIQ WLKDG GPSSG RPPPC
E11_SS/E11_2SH	D LSKQM EEECV RLYIQ WLKDG GPSSG RPPPC
E19_SS/E19_2SH	HGEG TFTSD LSKQM EEECV RLYIQ WLKDG GPSSG RPPPC

Figure 2. Nomenclature and sequence of synthesized peptides. Amino acid substitutions are indicated **in bold** in the sequences, while cysteines forming the disulfide bond are underlined.

The reduction of disulfide-bridge miniproteins was performed by TCEP or DTT reducing agents under neutral pH and varying conditions. COPASI 4.16 software was used to estimate the reduction kinetic parameters.

Far-UV range (FUV) ECD spectroscopy was used to monitor the temperature-dependent (5-85°C) native (F) → disordered (U) and time-dependent native (F) → amyloid (Amy) conformational transitions. I characterized the helical nature of each variant with ellipticity values

measured at 222 nm. ($|\Theta_{222nm}|$) With the two- ($F/U\%_{FUV}$) and three-component (F/U/Amy $\%_{FUV}$) deconvolution of the spectral series, the structural transitions could be quantified based on the ratio of the pure components. During the amyloid aggregation, the values of the three pure components as a function of time can be plotted in a barycentric coordinate system so the aggregation processes of E5 variants under different conditions can be described and compared.

The interaction of Tyr-Trp aromatic side chains in the central hydrophobic Trp cage of the miniproteins was investigated using near-UV (NUV) ECD spectroscopy in the course of temperature-dependent denaturation (Θ_{276nm}, Θ_{287nm}, Θ_{280nm}, Θ_{293nm}, $F\%_{FUV}$), amyloid aggregation and disulfide bridge reduction.

Based on the 2D homonuclear ^{1}H-^{1}H COSY, TOCSY, NOESY spectra, I performed the assignation and the determination of the 3D structure ensembles using Topspin 3.5 - 4.0.7, CCPNMR analysis V2.5, Aria 2.0.

Molecular dynamics simulations (MD), Dynamic light scattering (DLS), transmission electron microscopy (TEM), atomic force microscopy (AFM), and X-ray diffraction techniques (X-ray) were used to characterize the oligomerization process. MD, AFM, TEM and X-ray experiments were carried out by collaborators, the results were processed and summarized by me.

To determine the biological activity, we examined the insulin secretion-stimulating effect of miniproteins in mammalian INS-1E cell cultures. The concentration of the secreted insulin was determined by ELISA.

4. Results

A) I performed complete ^{1}H assignation of nine 25-amino acid long miniprotein variants **(figure 2.)** based on 2D homonuclear spectra at neutral pH at 5 different pharmacologically relevant temperatures. (4/15/26/37/48°C) Based on the NOESY type cross-peaks, I determined the structural ensembles of each state. **(figure 3.)** The thermal denaturation process of each variant was characterized by the number of assigned cross-peaks, the RMSD values of the backbone atoms of the structural population, and the RMSD values including all atoms along the sequence. With the secondary chemical shifts calculated from the chemical shifts, I quantified the folded content of the α-helical part and the Trp-cage compactness in each variant. I compared these NMR-derived values to the ellipticity values determined at each wavelength of the temperature-dependent (5-85 °C) ECD spectra and the ratio of the folded component determined from the deconvolution of the spectrum series. **(table 1.)** By bringing together the spectral parameters describing the fold of the miniprotein with the 3D structure ensembles, in addition to the illustration, the effect of the performed substitution on the spatial structure and thermal stability can also be quantified.

B) By analogy with the 25 amino acid long E5_A4C_E14D_S25C disulfide bridge cyclized peptide, I examined three different N-terminally truncated Exenatide derivatives. I determined and characterized the spatial structures of both the oxidized (SS) and their reduced (2SH) states according to the methods described in section 4/A at neutral pH and 15 °C. **(figure 4.)**

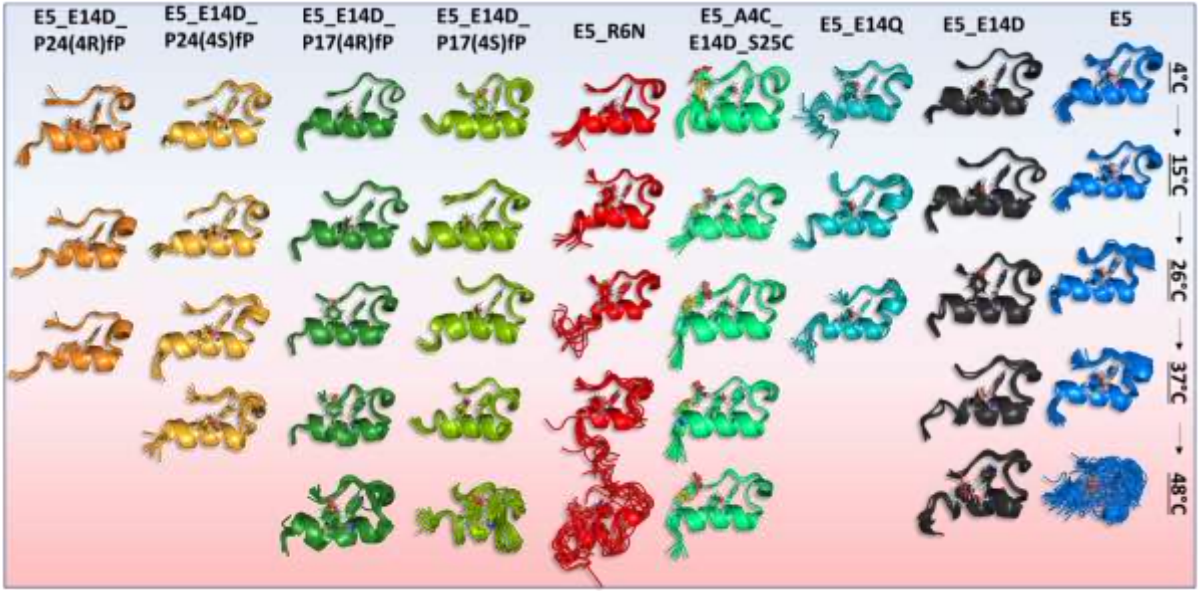

Figure 3. The 10-membered structures of the studied miniproteins as a function of temperature were determined by NMR spectroscopic methods.

Table 1. Spectral parameters describing the fold of the miniproteins

		Spectroscopiacal parameters								
		Helical propensities			Trp-cage prpoensities					
		$CSD_{Hdix\ 2-13}$	$\lvert\Theta_{222nm}\rvert$	F % H2V	CSD_{Tcage}	Θ_{274nm}	Θ_{287nm}	Θ_{280nm}	Θ_{298nm}	F % N2V
E5	4/5°C	3,37	17,90	76,20	9,14	4,79	1,60	4,43	-1,22	91,70
	10/11°C	3,47	16,80	73,10	8,74	4,64	1,68	4,45	-0,95	85,40
	25/26°C	3,39	15,25	67,90	8,12	4,29	1,71	4,41	-0,83	77,50
	37°C	3,15	13,49	58,15	7,13	3,71	1,78	3,72	-0,47	64,60
	48°C	2,67	11,81	48,70	5,74	2,72	1,23	2,78	-0,34	49,55
	85°C	n.d.	6,01	19,10	n.d.	0,10	-0,28	0,31	-0,54	6,60
E5_E14D	4/5°C	3,59	18,99	87,20	9,65	2,43	-0,08	1,95	-2,20	66,60
	10/11°C	3,63	18,25	82,10	9,35	2,55	0,29	2,38	-1,89	65,00
	25/26°C	3,58	16,71	76,00	8,83	2,50	0,40	2,25	-1,57	62,50
	37°C	3,35	14,34	63,10	7,90	1,98	0,35	1,90	-1,25	53,60
	48°C	2,87	11,79	49,25	6,41	1,55	0,38	1,34	-1,14	42,55
	85°C	n.d.	4,99	8,60	n.d.	-0,36	-0,80	-0,90	-0,92	3,30
E5_E14Q	4/5°C	3,19	15,64	67,20	8,23	4,18	1,34	3,95	-1,21	71,30
	10/11°C	3,19	14,51	62,20	7,70	3,89	1,56	4,00	-0,91	65,00
	25/26°C	3,06	12,20	54,80	6,95	3,46	1,33	3,33	-0,56	53,20
	37°C	2,74	10,77	43,60	6,01	2,49	1,12	2,52	-0,64	45,60
	48°C	n.d.	9,17	35,70	n.d.	2,00	0,99	2,09	-0,27	37,05
	85°C	n.d.	4,62	13,00	n.d.	0,15	-0,19	0,07	-0,38	2,60
E5_A4C_E14D_S25C	4/5°C	3,45	21,61	100,00	9,70	-2,03	-2,72	-1,91	-2,92	*
	10/11°C	3,58	20,81	97,50	9,60	-1,91	-2,61	-1,75	-2,73	*
	25/26°C	3,61	20,46	95,70	9,49	-1,91	-2,29	-1,72	-2,57	*
	37°C	3,65	19,46	92,30	9,33	-1,83	-2,00	-1,62	-2,33	*
	48°C	3,64	18,86	88,95	9,14	-1,70	-1,69	-1,47	-2,07	*
	85°C	n.d.	15,80	74,10	n.d.	-1,52	-1,09	-1,10	-1,40	*
E5_R6N	4/5°C	2,89	15,04	60,90	9,03	4,38	1,52	3,94	-0,93	84,00
	10/11°C	2,93	14,63	57,90	8,69	4,04	1,38	3,71	-0,82	79,10
	25/26°C	2,87	13,48	52,00	8,00	3,77	1,47	3,41	-0,48	71,50
	37°C	2,62	12,17	44,10	6,92	2,99	1,36	2,85	-0,37	64,05
	48°C	2,26	10,34	35,65	5,53	2,20	0,97	2,13	-0,31	46,15
	85°C	n.d.	6,26	10,90	n.d.	-0,33	-0,61	-0,55	-0,85	10,40
E5_E14D_P17(4S)fP	4/5°C	3,61	14,59	70,80	9,65	2,69	0,09	2,24	-1,51	98,60
	10/11°C	3,64	13,67	65,80	9,32	2,84	0,54	2,76	-1,30	93,70
	25/26°C	3,55	12,69	60,10	8,72	3,03	0,71	2,58	-0,92	82,90
	37°C	3,25	10,70	49,40	7,61	2,58	0,86	2,40	-0,56	68,80
	48°C	2,75	8,47	37,60	5,98	1,92	0,87	1,96	-0,36	52,05
	85°C	n.d.	3,92	8,10	n.d.	0,00	-0,06	0,14	-0,12	10,50
E5_E14D_P17(4R)fP	4/5°C	3,67	17,69	85,70	9,93	2,91	-0,24	2,26	-2,19	100,00
	10/11°C	3,73	17,43	81,40	9,69	2,93	-0,05	2,66	-1,90	95,70
	25/26°C	3,65	15,64	74,60	9,24	2,85	0,19	2,50	-1,47	88,80
	37°C	3,44	13,79	62,30	8,39	2,38	0,38	2,13	-1,11	76,10
	48°C	2,94	11,11	49,15	6,77	1,88	0,53	1,79	-0,77	60,60
	85°C	n.d.	4,36	8,70	n.d.	0,06	-0,30	-0,22	-0,53	13,10
E5_E14D_P24(4S)fP	4/5°C	3,43	16,11	76,50	9,48	4,51	1,24	4,00	-1,41	92,10
	10/11°C	3,53	14,92	69,20	9,21	4,58	1,54	4,35	-0,96	88,20
	25/26°C	3,45	13,55	63,20	8,71	4,44	1,55	4,11	-0,86	79,90
	37°C	3,23	11,39	51,05	7,80	3,59	1,53	3,45	-0,47	65,60
	48°C	n.d.	9,46	40,85	n.d.	2,92	1,33	2,64	-0,35	52,00
	85°C	n.d..	4,25	10,30	n.d.	0,21	-0,08	0,10	-0,26	8,20
E5_E14D_P24(4R)fP	4/5°C	3,48	13,88	66,80	9,21	1,92	-0,75	1,37	-2,81	68,90
	10/11°C	3,50	12,66	61,70	8,75	1,46	-0,50	1,63	-2,30	64,40
	25/26°C	3,35	10,99	53,70	7,93	1,54	-0,13	1,57	-1,71	58,00
	37°C	n.d..	8,80	41,40	n.d.	1,45	0,02	1,23	-1,07	46,00
	48°C	n.d..	6,54	30,80	n.d.	1,00	0,22	1,27	-0,78	33,20
	85°C	n.d.	2,46	10,00	n.d.	-0,17	-0,11	-0,19	-0,24	0,00

C) The SS→SH reduction of the miniproteins was monitored using ECD and ^{1}H NMR spectroscopy. Based on the signal integrals of the oxidized and reduced states in the 1D NMR spectra, I determined the reduction (k_1), oxidation (k_2) and aggregation (k_3) rate coefficients of each redox system under different experimental conditions using parameter estimation. Examining the mechanism of the reduction reaction, I gave a steric and electrostatic explanation for the significantly different reduction half-lives experienced for various miniproteins containing α-helixes of different lengths. **(figure 4.)**

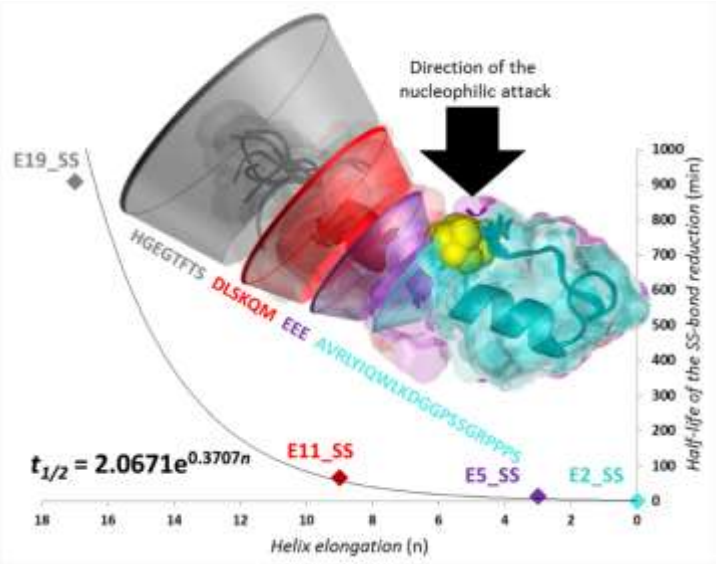

Figure 4. The half-life of disulfide bond reduction as a function of the length of the N-terminal α-helix. In the calculated 10-membered spatial structures, the cylindrical shells illustrate the steric shielding effect of the α-helix on the disulfide bridge (yellow spheres).

D) Despite the exceptional thermal stability of the disulfide bonded Exenatide analogue E19_SS, it has been shown to be a competitive antagonist by biological tests. **(figure 5.)**

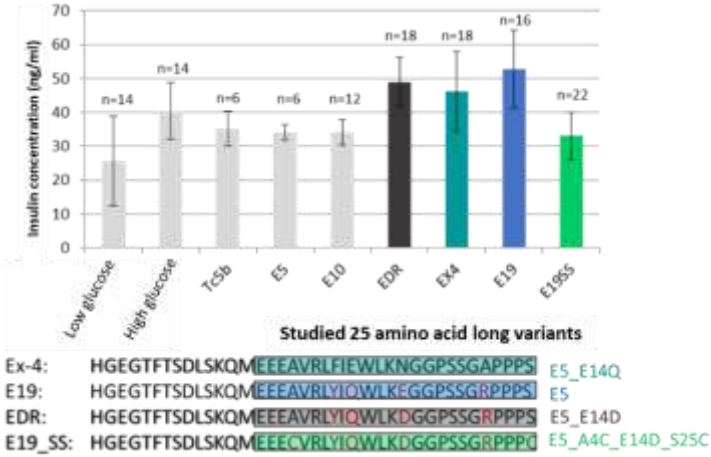

Figure 5. Results of biological activity tests. On each sequence, I highlighted the 25-amino acid long truncated analogs examined for temperature dependences in topic 4/A.

E) In the case of E5 miniprotein, amyloid formation showed pH and temperature dependence, and in the absence of agitation, only F→U transition was observed. In addition to increasing protein and NaCl concentrations, amyloid aggregation also occurred more rapidly. Intense amyloid aggregation was observed at the following (optimal) conditions: c_{E5} = 250 μM, c_{NaCl} = 50 mM, pH = 4.1, T = 37 °C with stirring.. To provide atomic-level model for the process, I investigated the pH and temperature dependence of the structure of E5. **(figure 6.)** Reversible aggregation was observed near the isoelectric point (pH 4-5), where despite the reduced

solubility, the molten-globule-like structure of E5 could be confirmed. At neutral and strongly acidic pH, the spatial the native Trp-cage motif was observed. **(figure 6.)**

Figure 6. E5 miniprotein pH (left) and temperature dependent (right) conformational changes. In the middle is the structure of the monomer that initiates amyloid aggregation, as well as a hypothetic amyloid fibril model. In the background are the applied spectroscopic methods.

F) The structural hoterogeneity of the calculated structures ensembles correlates with the number of possible microstates at a given pH. The different charge pattern of each microstate is determined by the pKa of the protonatable /deprotonable groups in the peptide sequence. Based on the 3D structures determined jointly by molecular dynamics simulations and NMR measurements, we identified the microstate that is most likely responsible for the formation of aggregation oligomers. Summarizing our results, I defined the spatial motifs that promote the association of the monomers.

G) The evolution of significant intermolecular aromatic-aromatic interaction could be observed during the aggregation process of E5 applying NUV spectroscopy. In addition, DLS was used to determine the size distribution of the samples (although due to the polydispersity of the aggregating system, these could only be interpreted with certain constraints. Based on these findings and on the AFM images of the aggregates, as well as the crystal structure of the peptide corresponding to the aggregation hot-spot of E5 (LYIQWL) and the results of molecular dynamics simulations, I proposed a structural model for the morphology of amyloid fiber state of E5. **(figure 7.)**

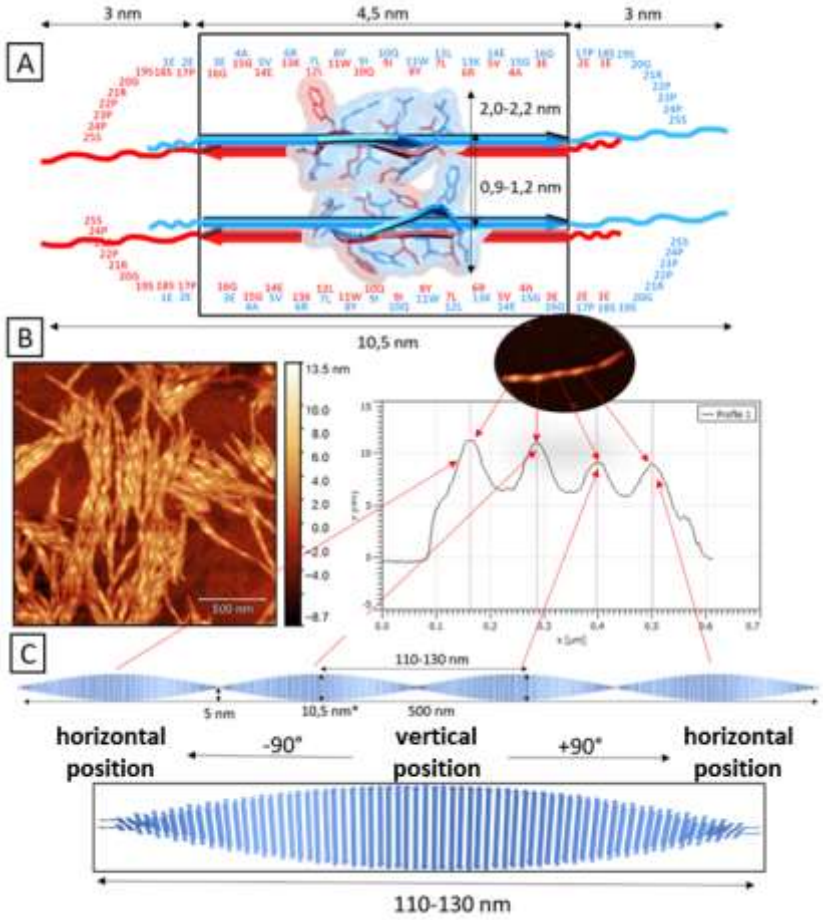

Figure 7. The putative E5 amyloid structure based on molecular dynamic simulations, AFM images, and X-ray crystallography. A) Schematic illustration of the β-sheet backbone (in frame) and the disordered C-terminals assumed on the basis of the crystal structure. B) -C) Harmonization between the AFM morphology of amyloid fibers after 72 h and the constructed amyloid model.

5. Conclusions

I observed a significant correlation between temperature-dependent NMR and FUV-ECD in parameters that describe the helicity and helical content. ($CSD_{helix\ 2\text{-}13}$; $[\Theta]_{222nm}$, F_{FUV}%) of miniprotein systems. The effect of sequential modifications on the structure is coherently by the changes of these values. For the parameters characterizing the quarterly spatial structure ($CSD_{cage,}$ $[\Theta]_{276nm}$, $[\Theta]_{287nm}$, $[\Theta]_{280nm}$, $[\Theta]_{293nm}$, F_{NUV}%), no correlation was observed between the values of the NMR and ECD data sets. Secondary chemical shift values correlate globally with the tertiary structural compactness of the tryptophan cage motif, whereas NUV-ECD describes more characteristically the spatial structure of aromatic side chains and their electron transitions.

Based on the determined 3D structural ensembles and spectroscopic results, it can be concluded that the the unfolding process of different E5 variants takes place by a similar mechanism where the native fold, only starts to loosen between 37 °C and 50 °C (F-U ratio 50-50%). Denaturation caused by temperature and pH changes loosens the Trp cage, which is a necessary but not sufficient condition for amyloid aggregation.

^{19}F substitutions of different prolines at γ position affect the stability and thermo-resistance of the Trp-cage motif in a sequence-specific manner. Enantiomer selective substitutions influence only the endo↔exo conformational equilibrium of the pyrrolidine ring to differing extent. I did not detect observable effect on the balance of cis-trans isomerism of the peptide backbone in the case of the studied ^{19}F-substituted peptides. At position 17P, the (4S) ^{19}F substitution decreases, while the (4R) substitution increases the structural order. At position 24P, both (4S) and (4R) reduce

thermal stability, but to a different degree. The observed differences may be due to the different efficiency of the hydration of the fluorine atom or its differing interaction with the aromatic side chains. Fluorine substitution delays but does not prevent amyloid aggregation.

I attributed the significant stability differences of E5, E5_E14D and E5_E14Q variants to the different compactness of the 3_{10}-helix due to the different H-bridge network and interactions between the side chains of Q10, X14, and R21. Neither the E14D nor the E14Q variant forms amyloid within the range of optimal amyloid formation conditions for E5. This demonstrates that amyloid aggregation can be inhibited under given conditions by well-chosen amino acid substitutions.

I showed that the R6N substitution of E5 promotes the unfolding process by destabilizing the α-helix, while the incorporation of the disulfide bridge completely prevents the disintegration of the tertiary structure. I found that by incorporating a well-placed disulfide bridge, the characteristic structure of the native Trp-cage can be irreversibly fixed over a wide temperature range (4-85°C) . This feature is extremely advantageous from the point of view of drug stability and formulation technology, since the peptide active ingredient can be applied under a wider range of shelf-life conditions.

However, in the case of E19_SS, binding to the extracellular domain of the GLP-1 receptor may occur based on literature data, however, the lack of increased insulin secretion supports the absence of receptor activation. The E19_SS construct also demonstrates that in the case of Exenatide-type incretin mimetics, the C-terminal region of the ligand must open during GLP-1R activation while proceeding into the binding pocket formed by transmembrane helices. Based on the biological test, the EDR variant proved

to be an agonist and, based on the thermal stability of the 25 amino acid E5_E14D derivative could be considered a potential drug candidate molecule.

The reduction of disulfide-bridge containing miniproteins proved to be a rather complex process. In addition to the reduction, the re-oxidation and aggregation also had to be taken into account to fully describe the events, which processes depend not only on the experimental parameters but also on the compactness of the molecule, the electrostatics environment of the disulfide bridge and the shielding effect of the α-helix on the disulfide bridge. I found NUV-ECD spectroscopy to be suitable for monitoring the disulfide bridge reduction within certain limitations. If Tyr / Trp is spatially close to the disulfide bridge, the reduction progress can be monitored by the change in intensity measured at 287 nm, while the kinetics of the entire redox system can be described by NMR spectroscopy based on the time-dependent ^{1}H signal integrals of the oxidized and reduced forms. Reduction experiments performed under different experimental conditions shed light on the effect of commonly varied parameters on reduction kinetics.

I demonstrated that the number of protonation microstates found at each pH value correlates with the heterogeneity of the NMR-derived structure ensembles, also reflected in the increased RMSD values. I concluded that initiation of the nucleation processes of amyloid aggregation require the increased exposition of the hydrophobic side chains (opening of the Trp cage), and a such charge distribution along the sequence that supports intermolecular interactions. This was also supported by the results of molecular dynamic simulations carried out by my co-workers.

The ordered α-helix (F) → disordered (U) → β-sheet (Amy) amyloid transformations during the oligomerization and subsequent elongation processes of amyloid formation can be followed and quantified by deconvolution of the FUV-ECD spectral series. I showed that plotting the time-dependent ratio of each pure component (F/U/Amy) in a barycentric coordinate system can be monitor the effect of sequence variations and different external conditions ($c_{fehérje}$, c_{NaCl}, *pH*, *T*, stirring) – providing a straightforward methodology that may support the design of peptide medications that remain stable under both relevant laboratory- and physiological-conditions . With solution-state NMR techniques, only conformational changes in the monomer can be detected, the oligomers remain invisible due to their size and heterogeneity. The partial information obtained from the parallel applied biophysical methods provides only an approximate picture of the initial stage of aggregation and the size distribution of the oligomers.

In the amyloid-like crystal grown from the LYIQWL sequence of the E5 miniprotein, the β-strands are antiparallel, and the β-layers pair in a equifacial manner, so they can be classified into the 8th class according to the Eisenberg amiloid classification. The opposing β-strands perpendicular to the longitudinal axis of the amyloid fiber are parallel in pairs and form a common surface with the matching sidechains. In the amyloid model E5, from Glu 3 to Gly 16, presumably, the entire sequence forms a linear β-strand similar to that in the amyloid structure of sequentially homologous glucagon. The antiparallel β-strand lined along the longitudinal axis of the amyloid fiber form an angle of 0.75 ° with each other, resulting in a twisted morphology.

Publications

Publications pertaining to the doctoral thesis:

1) Horváth, D., Taricska, N., Keszei, E., Stráner, P., Farkas, V., Tóth, G. K., & Perczel, A. (2020). Compactness of Protein Folds Alters Disulfide-Bond Reducibility by Three Orders of Magnitude: A Comprehensive Kinetic Case Study on the Reduction of Differently Sized Tryptophan Cage Model Proteins. *Chembiochem: a European journal of chemical biology*, *21*(5), 681–695.
2) Taricska, N., Horváth, D., Menyhárd, D. K., Ákontz-Kiss, H., Noji, M., So, M., Goto, Y., Fujiwara, T., & Perczel, A. (2020). The Route from the Folded to the Amyloid State: Exploring the Potential Energy Surface of a Drug-Like Miniprotein. *Chemistry*, *26*(9), 1968–1978.
3) Horváth, D., Menyhárd, D. K., & Perczel, A. (2019). Protein Aggregation in a Nutshell: The Splendid Molecular Architecture of the Dreaded Amyloid Fibrils. *Current protein & peptide science*, *20*(11), 1077–1088.